



# Experimental noise source identification in a fuselage test environment based on nearfield acoustical holography

S. Ungnad<sup>1</sup> · D. Sachau<sup>1</sup> · M. Wandel<sup>2</sup> · C. Thomas<sup>2</sup>

Received: 22 February 2021 / Revised: 23 July 2021 / Accepted: 28 July 2021 / Published online: 18 August 2021  
© The Author(s) 2021

## Abstract

A major challenge in the subject of noise exposure in airplanes is to achieve a desired transmission loss of lightweight structures in the low-frequency range. To make use of appropriate noise reduction methods, identification of dominant acoustic sources is required. It is possible to determine noise sources by measuring the sound field quantity, sound pressure, as well as its gradient and calculating sound intensity by post-processing. Since such a measurement procedure entails a large amount of resources, alternatives need to be established. With nearfield acoustical holography in the 1980s, a method came into play which enabled engineers to inversely determine sources of sound by just measuring sound pressures at easily accessible locations in the hydrodynamic nearfield of sound-emitting structures. This article presents an application of nearfield acoustical holography in the aircraft fuselage model Acoustic Flight-Lab at the Center of Applied Aeronautical Research in Hamburg, Germany. The necessary sound pressure measurement takes one hour approximately and is carried out by a self-moving microphone frame. In result, one gets a complete picture of active sound intensity at cavity boundaries up to a frequency of 300 Hz. Results are compared to measurement data.

**Keywords** Nearfield acoustical holography · Inverse acoustics · Microphone · Sound intensity

## 1 Introduction

In many practical situations, the measurable acoustic radiation of sound pressure does not allow to draw conclusions about sound sources producing unwanted noise. In the case of an aircraft cabin, this instance can be due to reflections. To find those dominant radiating surface segments, called sources, an acoustic intensity measurement would have to be carried out in the entire cabin. Thus, to determine dominant noise sources with a reasonable measurement effort, new procedures of noise source identification are required. In this article, a method based on nearfield acoustical holography (NAH) is being investigated in application to a cylindrical approximation of an aircraft, the Acoustic Flight-Lab (AFL), at the Center of Applied Aeronautical Research in Hamburg, Germany.

### 1.1 Problem statement

The elimination or reduction of noise sources is a major concern of the automobile, aircraft, appliance and machine manufacturers. As a result, understanding the causes of noise generation can significantly improve product performance. The diagnosis of noise due to vibration begins with measurement of sound and vibration quantities. However, in a complicated measurement environment, it can be difficult to gain information about noise sources because of inaccessible measurement locations. Usually, a lack of information between vibrations and the resulting radiation of sound pressure is in place when applying conventional measurement methods based on accelerometers, microphones or sound intensity probes. In addition, limited resources often lead to local measurements, whereby information about the sound field is obtained at certain locations and no overall picture of the acoustic environment can be obtained. Finally, measured values that are uncorrelated to the actual sound source due to many reflective surfaces pose additional challenges.

In the present application, the primary structure is covered by insulating material, except of the floor panels, which prevents the attachment of accelerometers and measurements

✉ S. Ungnad  
ungnads@hsu-hh.de

<sup>1</sup> Helmut-Schmidt-Universität/Universität der Bundeswehr Hamburg, Holstenhofweg 85, 22043 Hamburg, Germany

<sup>2</sup> Airbus Operations GmbH, Kreetzslag 10, 21129 Hamburg, Germany

by laser Doppler vibrometry. Furthermore, sound sources over the entire cabin should be determined, which means that a sound intensity measurement involves a disproportionately large amount of resources.

## 1.2 Solution approach

The stated difficulties can be tackled using methods of inverse sound source reconstruction. Here, on the basis of a mathematical sound radiation model, an overall picture of acoustic sinks and sources in the stationary sound field can be created. The choice of the mathematical model depends on the acoustic environment. Since the investigations take place in the frequency range  $< 300$  Hz, a modal approach for calculating the sound propagation in the aircraft cavity should serve as a model assumption. For irregularly shaped geometries, the finite element method (FEM) is an appropriate possibility to calculate the required modal quantities in the form of pairs of eigenvalues and eigenvectors. Thus, it is used here in application to a sound field inside the aircraft mock-up AFL.

## 1.3 State-of-the-art

First progress on inverse methods is documented in the subject of image processing in [1]. Nowadays, these methods are still in use. They form the basis for computer tomography. Since the work in [2], it is known that the properties existence, uniqueness and convergence of an inverse mathematical solution always need to be clarified to check if it is ill-posed. The question of ill-posed problems further leads to the subject of regularization. Subsequent to the growth of applications in image processing, inverse methods improving electron microscopy in [3] form the basis for optical holography based on Fourier optics, which is summarized in Chapter 9 in [4]. Analogous to visual abilities, separate light sources are used here to detect objects by measuring the coherent distribution of the scattered wave field. An inverse formulation for planar radiators is documented in [5]. By transferring this method to acoustics, which is summarized in [6], one comes across with the far-field resolution limit. Next, if sound-emitting structures are considered and no source of acoustic “illumination” is used, the interpretation of the inverse diffraction problem changes. Both steps lead to the development of NAH in [7]. Therefore, the inverse formulation is transferred from optics to acoustics [8], while the measurement positions are adapted to the issue of acoustical resolution by moving into the hydrodynamic nearfield, as defined in [9]. Understanding about the fact that inverse versions of already existing acoustic computation methods, like Fourier acoustics, in combination with nearfield measurements form a powerful tool of source identification leads to further progress in NAH. Accordingly, a variety of

NAH methods exist which are based on different mathematical models. Besides the Fourier-transform, these methods comprise the boundary element method [10], the Green’s function method [11], the Helmholtz equation least-squares method [12], transfer function methods [13] with transition to beamforming [14] and aero-acoustic measurements [15], the equivalent source method [16], Bayesian focusing [17] and the FEM [18]. The application scenario determines which model is used. Measured transfer paths can replace mathematical models, but the measurement effort can be disproportionate. Since NAH methods often use microphone arrays, it is sometimes necessary to distinguish between sources on both sides of the array which can be due to reflections. Accordingly, double-layer imaging techniques for the characterization of sound sources in confined spaces have been developed [19, 20]. For the application of inverse sound source reconstruction in an aircraft test environments valuable remarks concerning vibro-acoustic properties of such cylindrical structures can be taken from [21]. Fruitful applications of sound field reconstruction methods in flight can be found in [22–24]. More recent examples in [25–28] show that NAH methods can be used in a complementary way to methods like beam-forming, intensity measurements, transfer path and panel contribution analysis when dealing with sound fields in vehicles, especially when a global picture of sound sources is requested.

## 1.4 Objectives

The FEM-based NAH in [18] is used here for interior noise source identification on the basis of inversely identified sound field quantities at cavity boundaries. For the present single aisle mock-up structure with point force excitation, methodological refinements concerning eigen-solutions with Neumann and Dirichlet boundary conditions are necessary. In contrast to preliminary works in [18], the aim is to determine sound intensities upon the surface of insulation material covering the primary structure. In a preceding step, reconstructed particle velocities on floor panels will be compared to measured structural velocities to evaluate occurring errors involved in the inverse procedure.

## 2 Measurement environment

The AFL test rig in Fig. 1 has a total length of approximately 8.5 m and is further explained in [29]. Inner acoustic foam wedges generate a free-field-like boundary condition in x-direction. An electromagnetic shaker excites the stiffened cylindrical structure by a random noise signal. A schematic representation of the test environment is found in Fig. 2. The AFL is closed at its front and back by muffling caps. The microphone array for the NAH measurements is attached to

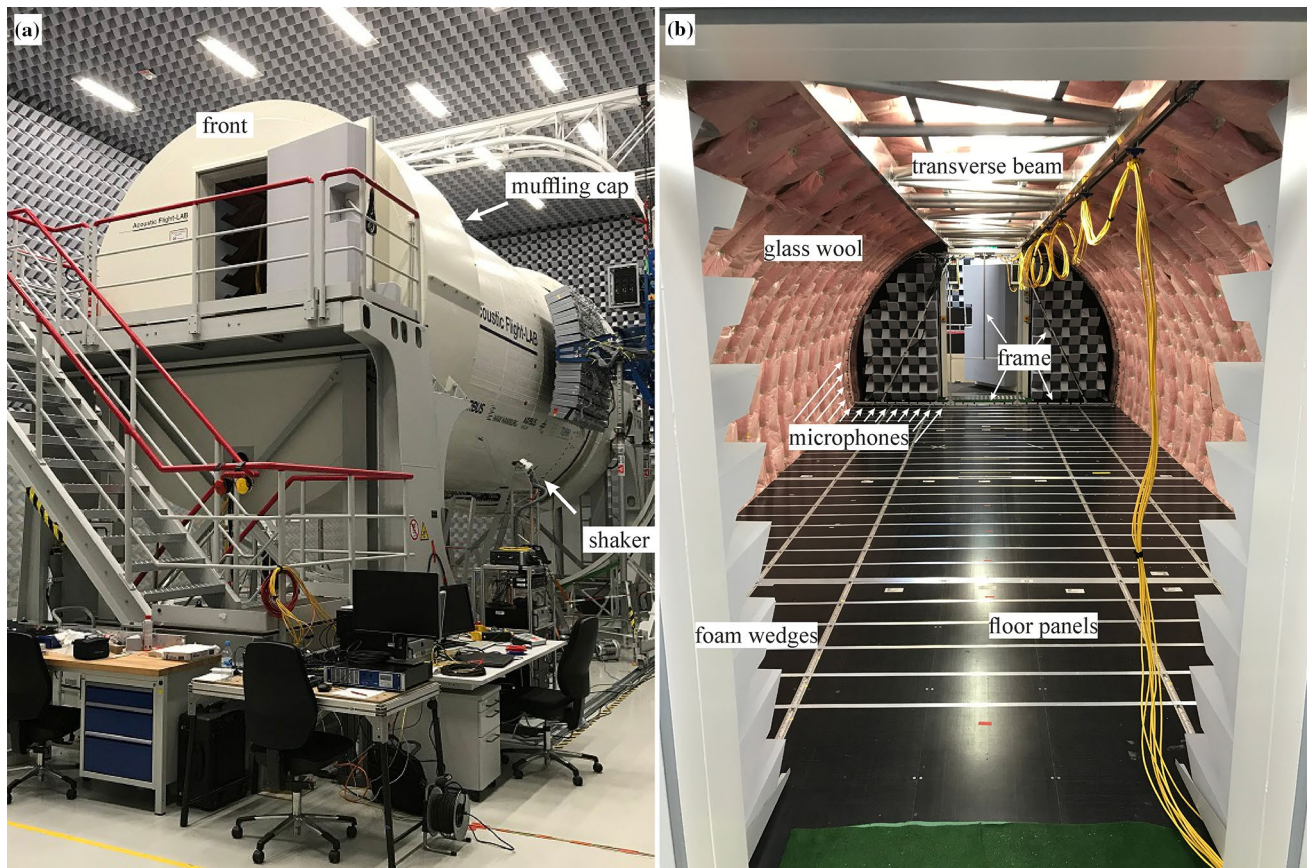


**Fig. 1** Measurement environment—**a** overall view of the cylindrical aircraft cabin mock-up AFL with muffling caps at the front and at the back; excitation is realized by an electromagnetic shaker; loudspeakers are not used; **b** inner view of the cabin

a transverse beam which is not connected to the structure. The microphone frame can be moved automatically using a stepper motor.

## 2.1 Microphone positions

The microphone positioning depends on the smallest bending wavelength to be reconstructed on the structure. Other influencing factors such as the dynamic range of the measurement set-up are treated in [18]. The highest frequency to be considered results from the selected modal approach in the following section. If the diameter of the cylindrical AFL is taken as characteristic length and a low acoustic modal density by means of a maximum tolerated acoustic Helmholtz number of three according to chapter 9 in [30], the cut-off frequency of 260 Hz results. At 260 Hz, the structural waves occurring result from local structural response superimposed on global structural modes, see figure 6 in [31]. Accordingly, structural wave lengths can be assigned to the low-frequency range ( $< 160$  Hz) and to the mid-frequency range between 160 and 260 Hz, as introduced in [21]. The shortest wavelength appearing in the measurement data has

a length of approximately 0.3 m. To meet the Nyquist–Shannon sampling theorem, microphones are installed in a distance of 0.15 m to each other on the measurement frame. A configuration with 65 microphones conformal to the structure's boundaries in Fig. 3 is chosen. In that figure, the model boundaries coincide with the mock-up's aluminum skin and with floor panels which surround the contained air volume. Microphone positions are marked with black dots.

The chosen number of microphones offers a compromise between total weight of the microphone frame, cabling effort and resolution of the inner sound pressure field. The prerequisite for this decision is that the microphones at the edge contain the information about the internal sound field with a sufficiently high density of measurement positions and therefore no further microphones are required in the middle of the cavity. This fact results from Sect. 4.3. in [32], in that, the calculation of a sound field with given geometry is solely possible through sound pressures at its boundary. Therefore, it is assumed that any sound field can be calculated by a complete set of eigen-functions which fulfill pre-defined boundary conditions. In the following description, Neumann and Dirichlet boundary conditions are necessary.



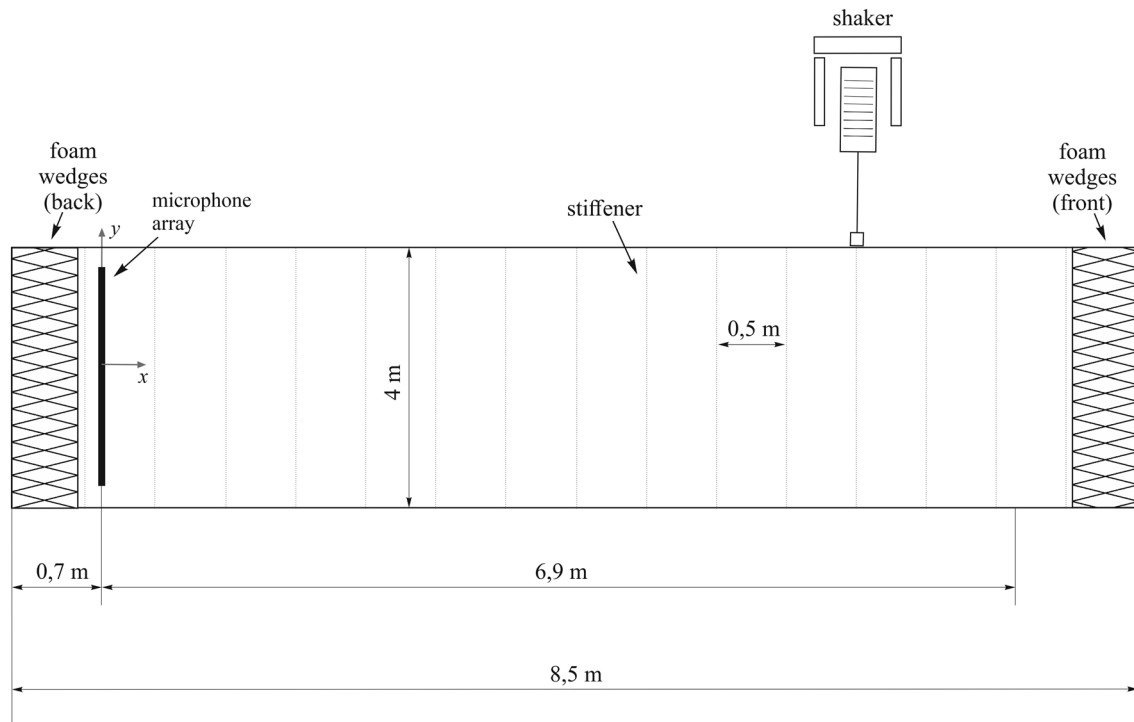
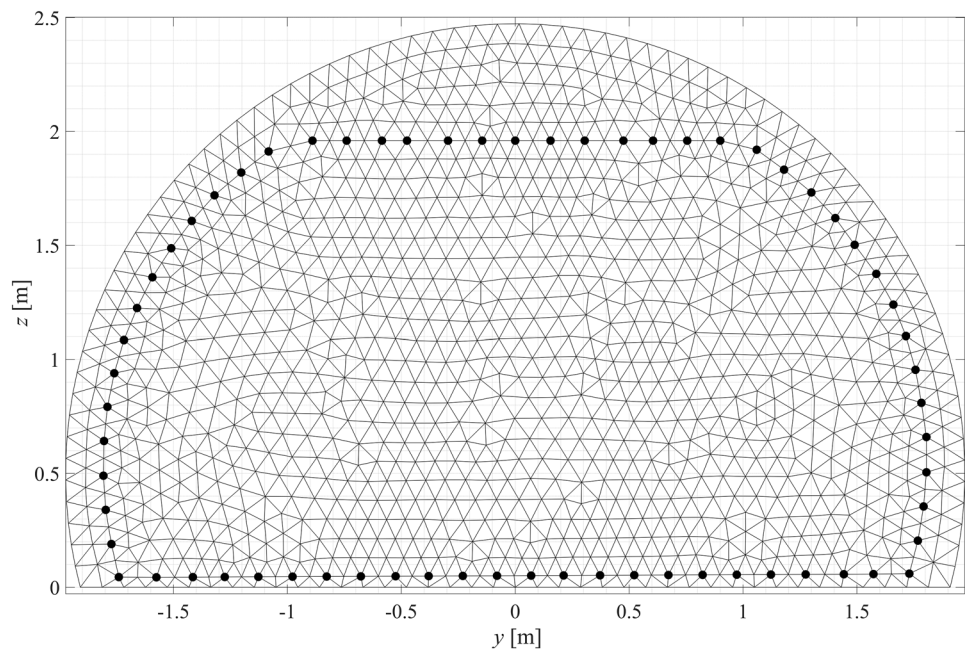


**Fig. 2** Schematic of the measurement environment in the cylindrical aircraft mock-up made from aluminum; a conformal microphone array consisting of 65 microphones of type Brüel & Kjær

4958 is moved in x-direction automatically to measure the response due to the excitation by the electromagnetic shaker of type TIRA S51120MOSP

**Fig. 3** Microphone positions (black dots) displayed on a finite element mesh at a frequency of 70 Hz; the bottom measuring row slightly deviates from its conformal state because of uncertainties during installation; the maximum element size is chosen with a twelfth of the acoustic half-wavelength



## 2.2 Measurement procedure

With an array step size of 0.15 m designed in the previous section, the length of the measurement region is 6.9 m. Consequently, there are 47 positions in total the microphone

array moves to inside the mock-up. Time data recording is conducted with reference impedance sensor between the structure and the electromagnetic shaker. According to [21], the shaker is attached to a stiffener to achieve the desired structural response in the intended frequency range. The

frequency response is calculated according to chapter 7.3 in [33] with a sampling frequency of 8192 Hz. An overlap between time data blocks of 95% and Hann-windowing is applied. The signal-to-noise ranges from 30 to 40 dB. The result of the sound pressure measurement is presented for the frequency of 90 Hz in Fig. 4. The loudspeakers in Fig. 2 are not used.

These measurement data form the input variable for the inverse method described in the following section.

### 3 NAH method based on finite elements

FEM-based NAH grounds on the fact that the acoustic transfer matrix between particle velocities at cavity boundaries and sound pressures at microphone positions is calculated. Hereafter, the transfer matrix is inverted and multiplied by measured sound pressures. The calculation is carried out according to [18] with the approach of combining the two-dimensional finite element model in Fig. 3 with one-dimensional analytical model. The assumption made here is that the cross section of the AFL does not change.

Circular eigen-frequencies  $\omega^{2D}$  of the two-dimensional model in Fig. 3 are the entries on the main diagonal of  $\Omega^{2D} \in \mathbb{R}^{E \times E}$ , where  $\Omega^{2D}$  calculates according to Equation 9.41 in [34]:

$$\Omega^{2D} = \sqrt{\Psi^{2D^T} \mathbf{K}^{2D} \Psi^{2D}}. \tag{1}$$

$\mathbf{K}^{2D} \in \mathbb{R}^{N \times N}$  and  $\Psi^{2D} \in \mathbb{R}^{N \times E}$  represent the stiffness and the projection matrix of the two-dimensional finite element model. (...) <sup>T</sup> marks a matrix transpose.  $N$  is the number of degrees of freedom of the model with linear basis functions. The variable  $E$  labels the number of eigen-solutions

resulting from the eigenvalue problem, which contains the natural boundary condition of a vanishing pressure gradient:

$$(\mathbf{K}^{2D} - \mathbf{M}^{2D}(\Omega^{2D})^2)\Psi^{2D} = 0. \tag{2}$$

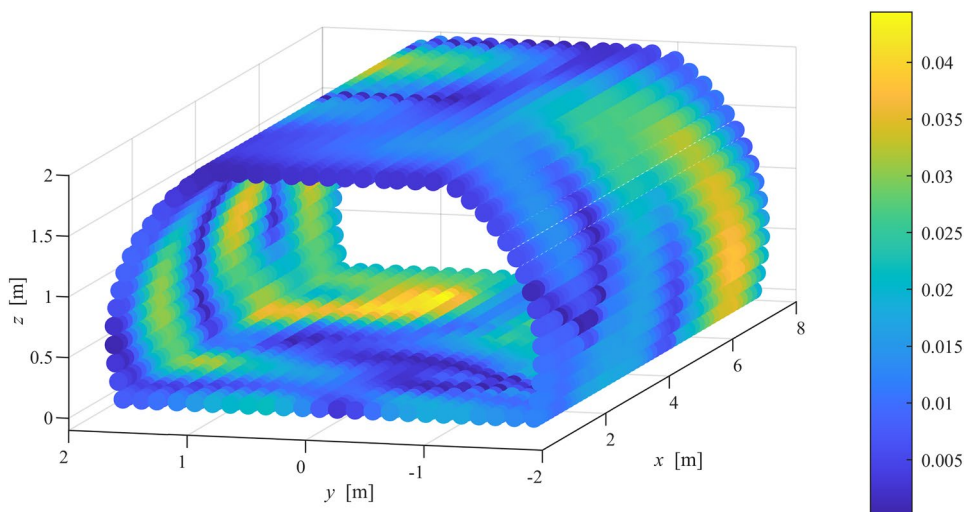
Here,  $\mathbf{M}^{2D} \in \mathbb{R}^{N \times N}$  is the mass matrix. The wavenumber eigen-solutions of the complete cavity  $k_n$  calculate with:

$$k_n = \sqrt{\frac{(\omega_l^{2D})^2}{c^2} + \left(\frac{m\pi}{L}\right)^2}. \tag{3}$$

$c$  is the speed of sound. Indices  $l$  and  $m$  are chosen in a way, that the  $l$ th eigen-frequency of the two-dimensional model and the  $m$ th analytic eigen-frequency of a one-dimensional standing wave with length  $L$  and Dirichlet boundary condition are projected on the single index  $n$  assigned to the wavenumber  $k_n(l, m)$  in ascending order, namely  $0 \leq k_1(l, m) \leq k_2(l, m) \leq \dots \leq k_n(l, m)$ . Thus, pairs of eigen-values and eigenmodes can be generated for a three-dimensional model of the AFL cavity. The number of eigen-solutions  $E$  is chosen depending on the frequency. It is chosen in a way that the highest modal wavenumber  $k_n$  does not exceed the triple of the acoustic wavenumber [18]. Cavity recesses caused by inwardly protruding stiffeners or components of the microphone array are neglected. The resolution of the element nodes at the cavity boundaries should be chosen in a way that the mean element edge length  $\bar{L}$  is smaller than the smallest half-wavelength that occurs on the structure. Consequently  $\bar{L}$  is frequency-dependent. It is chosen to be constant and a fraction of  $L$ . The eigenmodes  $\Psi_n \in \mathbb{R}^{N(\frac{L}{\bar{L}}+1) \times 1}$  calculate according to the sound soft boundary condition:

$$\Psi_n(l, m) = \Psi_l^{2D} \otimes \sin\left(\frac{m\pi x}{L}\right). \tag{4}$$

**Fig. 4** Sound pressure distribution from absolute values of frequency response data; this forms the basis for the subsequent inverse calculation; frequency 90 Hz; color bar in units of [Pa/V]



Again, the index  $n$  is assigned to pre-sorted wavenumber eigenvalues  $k_n$  of the three-dimensional cavity model.  $\Psi_l^{2D} \in \mathbb{R}^{N \times 1}$  represents an eigenmode in the  $l$ 'th column of  $\Psi^{2D}$ .  $\otimes$  represents the outer product and  $\bar{\mathbf{x}} \in \mathbb{R}^{\left(\frac{L}{\bar{L}}+1\right) \times 1}$  comprises a sampled version of the coordinate  $x$  with sampling interval  $\bar{L}$ :

$$\bar{\mathbf{x}} = \left[ 0, \bar{L}, 2\bar{L}, \dots, L - \bar{L}, L \right]^T. \quad (5)$$

Hence, one can be sure that the resolution in  $x$ -direction matches the element edge length  $\bar{L}$  of the two-dimensional model. Through selection of  $M$  measurement nodes and  $B$  boundary nodes in  $\Psi_n$  the acoustic transfer matrix  $\mathbf{Z}$  is given with:

$$\mathbf{Z} = -j \frac{2\omega\varrho}{L} \sum_{n=1}^E \frac{\hat{\Psi}_n \check{\Psi}_n^T}{(k_n^2 - k^2)}. \quad (6)$$

Here,  $\omega$  and  $k$  are the circular frequency and the wavenumber. The complex number is defined with  $j = \sqrt{-1}$ . The density of air is labeled with  $\varrho$ .  $\hat{\Psi}_n \in \mathbb{R}^{M \left(\frac{L}{\bar{L}}+1\right) \times 1}$  and  $\check{\Psi}_n \in \mathbb{R}^{B \left(\frac{L}{\bar{L}}+1\right) \times 1}$  result, if just measurement nodes or boundary nodes are taken into account. For the purpose of inverse reconstruction of particle velocity, singular value decomposition of  $\mathbf{Z}$  according to [35] gives:

$$\mathbf{Z} = \mathbf{U}\mathbf{\Sigma}\mathbf{V}^H. \quad (7)$$

Here, the mathematical operator  $(\dots)^H$  produces a complex conjugate matrix.  $\mathbf{U} \in \mathbb{C}^{M \times M}$  and  $\mathbf{V}^H \in \mathbb{C}^{B \times B}$  represent unitary matrices comprising so-called singular modes in their columns. Singular values are available on the diagonal of  $\mathbf{\Sigma} \in \mathbb{R}^{M \times B}$ . For over-determined systems of equations considered here, the pseudoinverse  $\mathbf{Z}^\dagger$  according to [36] calculates with:

$$\mathbf{Z}^\dagger = (\mathbf{Z}^H \mathbf{Z})^{-1} \mathbf{Z}^H. \quad (8)$$

Inserting Eq. (7) in Eq. (8) yields:

$$\mathbf{Z}^\dagger = \mathbf{V}(\mathbf{\Sigma}^T \mathbf{\Sigma})^{-1} \mathbf{\Sigma}^T \mathbf{U}^H. \quad (9)$$

This equation generates an inverse propagator for the reconstruction of particle velocities  $\mathbf{v}$  at cavity boundaries of the AFL based on the measured sound pressures in  $\mathbf{p}$ :

$$\mathbf{v} = \mathbf{Z}^\dagger \mathbf{p}. \quad (10)$$

Equation (10) is ill-posed because it contains small values on the main diagonal of  $\mathbf{\Sigma}^T \mathbf{\Sigma}$ . This amplifies the measurement errors in  $\mathbf{p}$ , which are interpreted by Eq. (10) as physically meaningful. It is possible to suppress error amplification by regularization procedures like Tikhonov's regularization in [37]. Therefore, numerical noise

represented by small singular values in  $\mathbf{\Sigma}^T \mathbf{\Sigma}$  and associated singular modes is attenuated using the regularization parameter  $\mu$ . Thus, the smoothed solution  $\tilde{\mathbf{v}}$  is given with:

$$\tilde{\mathbf{v}} = \mathbf{V}(\mathbf{\Sigma}^T \mathbf{\Sigma} + \mu^2 \mathbf{I})^{-1} \mathbf{\Sigma}^T \mathbf{U}^H \mathbf{p}. \quad (11)$$

It is important to note that smoothing always is accompanied by biases. With an appropriate value of  $\mu$ , one tries to find a balance between these two influencing factors. A procedure of finding a  $\mu$  that suits the expected solution is the L-curve method, documented in [38]. This method makes use of a double logarithmic visualization of the Euclidean solution norm  $\tilde{\mathbf{v}}(\mu)$  against the residual norm  $\mathbf{U}\mathbf{\Sigma}\mathbf{V}^H \tilde{\mathbf{v}}(\mu) - \mathbf{p}$ , where the transition between over-smoothing and error amplification is chosen to define  $\mu$ . This procedure is also used in the following chapter for the purpose of regularization.

## 4 Results

Results are presented in two steps. First, inversely reconstructed particle velocities and measured structural velocities are displayed above the floor of the AFL. The latter are measured by the German Aerospace Centre using laser Doppler vibrometry with a measurement resolution comparable to that in Sect. 2.1. Second, the active sound intensity is evaluated on the boundaries of the entire cavity.

### 4.1 Inverse particle velocity vs. measured structural velocity

To compare inverse results with measurements, real parts of velocities normal to floor panels are presented for two different frequencies on a photograph in Figs. 5 and 6. The photograph is taken from the rear wedges towards the front (see Fig. 2). The cylindrical structure is excited into vibration from the outside with an electromagnetic shaker placed on the left in the direction of the front door at the level of the floor panels. To present the deviation between measured and inversely reconstructed data, the root mean square of velocities over all measurement positions is given in Fig. 7. Accordingly, the smoothing effect of  $\mu$  in Eq. (11) is noticeable below 220 Hz.

All the data displayed are normalized to the reference voltage signal of the force sensor in the impedance head of type PCB 288D01. The amplitudes of the measurements and the calculations agree well. Inverse results provide "smoother" velocity fields compared to the measurement data, because acoustic modes with low-phase velocity are smoothed by Eq. (11). As already mentioned, this regularization step creates a compromise between falsification and smoothing. At

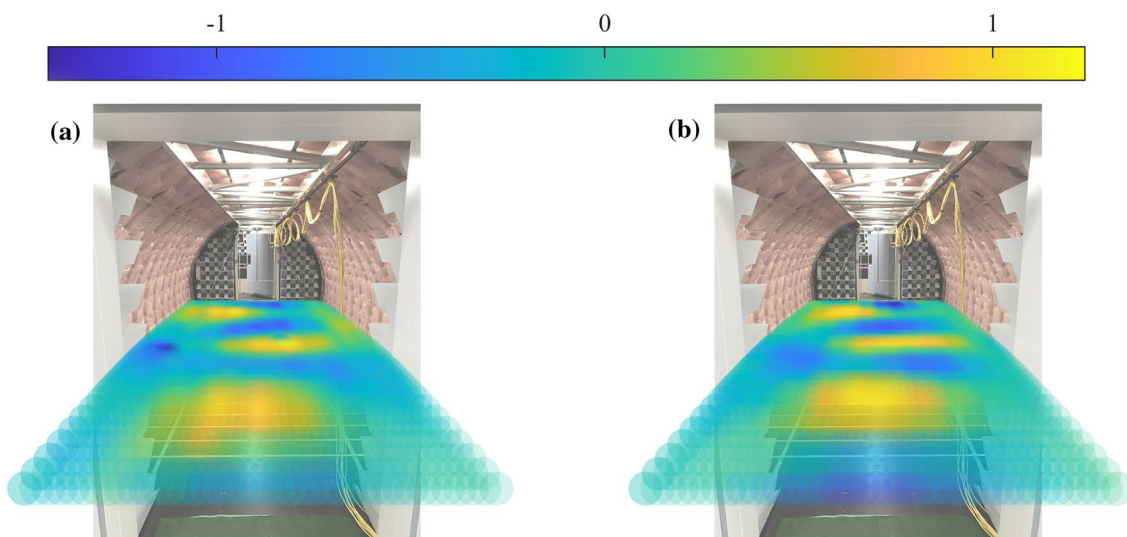


**Fig. 5** Comparison at 80 Hz of **a** measured structural velocities and **b** inversely calculated particle velocities on the surface of the floor panels in linear scale; the real part of the normal velocity component is depicted on a photograph of the AFL cabin; color bar in units of  $[10^{-4} \text{ m/Vs}]$

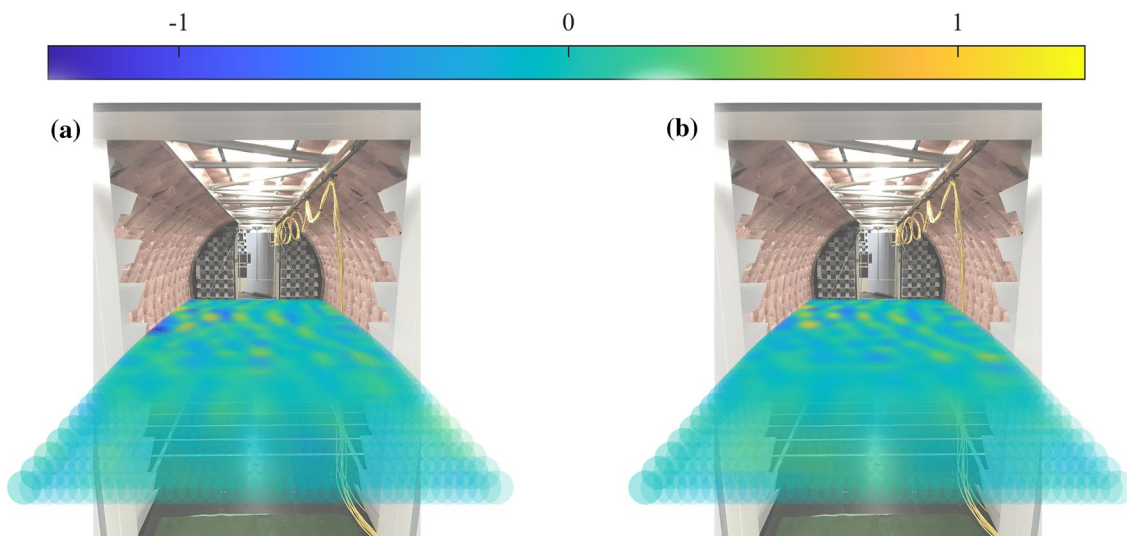


**Fig. 6** Comparison at 260 Hz of **a** measured structural velocities and **b** inversely calculated particle velocities on the surface of the floor panels in linear scale; the real part of the normal velocity component is depicted on a photograph of the AFL cabin; color bar in units of  $[10^{-4} \text{ m/Vs}]$

a frequency of 260 Hz, the propagation of structural waves from the point of excitation is visible.

### 4.2 Sound intensity on cavity boundaries

The validation of the NAH based on FEM comparing the structural and reconstructed particle velocity is followed by the evaluation of the active sound intensity. This in turn provides valuable information about present sources of noise in the AFL cabin. The calculation of the necessary boundary sound pressures is carried out via the acoustic

transfer matrix in Eq. (6). Results are again related to the reference signal. In Fig. 8, the sound intensities perpendicularly directed to the boundaries are displayed at the frequency of 121 Hz. Accordingly, a large proportion of sound energy (in yellow) enters the cavity near the point of excitation, but “phantom” sources also occur. Both effects strongly depend on the frequency considered. According to Sect. 4.8.4 in [39], the sound intensities can be averaged over time and third octave bands, which is shown in Fig. 9. With increasing frequency, the amplitude maxima of sound intensities concentrate at the point of force



**Fig. 7** Root mean square of the measured structural velocities and of the inversely reconstructed particle velocities over all measurement points on the floor panels

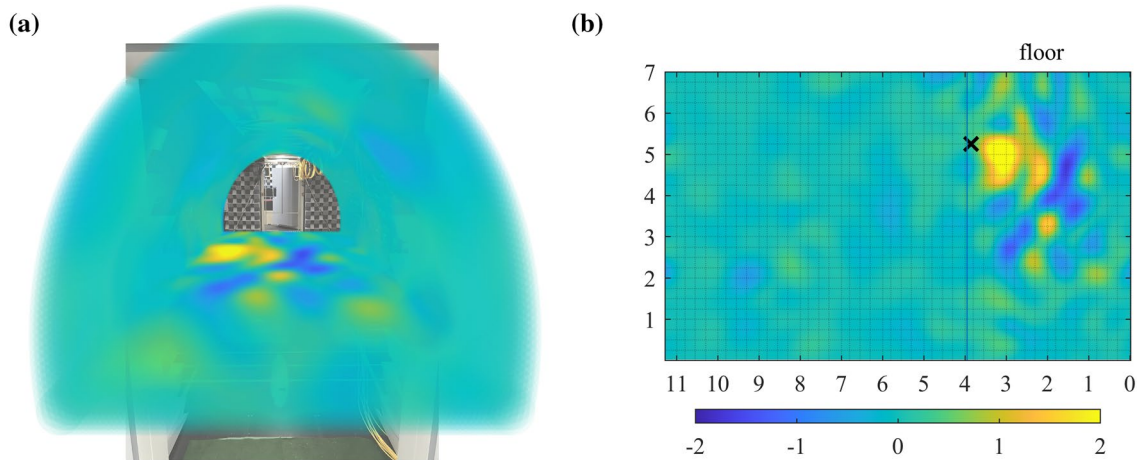
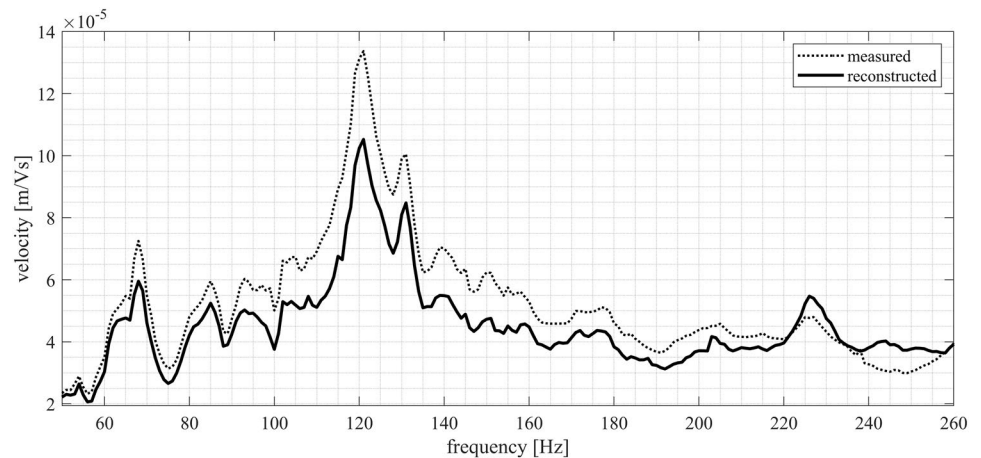


**Fig. 8** Perpendicularly directed time-averaged sound intensities; **a** three-dimensional view; **b** two-dimensional view; frequency 121 Hz; the point of excitation is marked by a cross; color bar in units of  $[10^{-6} \text{ W/m}^2\text{V}^2]$

excitation, while the transition from global to local energy transport is noticeable, which is in accordance with observations made in [31]. Nevertheless, in part (b), one could not find the excitation point, due to phantom sources. With increasing frequency, the response on floor panels dominates the transmission of acoustic energy, which is to be expected, since no insulation material covers that region.

In the example presented in Fig. 8, the number measurement nodes  $M$  is chosen with 3055, which is kept constant over all frequencies, since this is the total number of measurement positions. However, the number of boundary nodes  $B$ , the number of degrees of freedom  $N$  and the number of considered eigen-solutions  $E$  are frequency-dependent. At the frequency of 121 Hz, the method in Sect. 3 inversely calculates the sound intensity with  $B = 1739$ ,  $N = 648$  and  $E = 426$ , which results in a

post-processing time of 10 s using a desktop PC with 32 GB RAM and a tenth generation i7 processor.

## 5 Conclusion

An experimental application of the FEM-based NAH for reconstructing sound field quantities at the boundaries of a full-scale fuselage structure is realized. Measurement of the inner sound pressure field and acoustic transfer functions of a two-dimensional finite element model in combination with a one-dimensional standing wave are utilized. After checking the inverse results against vibrometer measurements, a complete picture of the noise transmission through the cabin wall is obtained by determining the time-averaged sound intensity upon the surface of



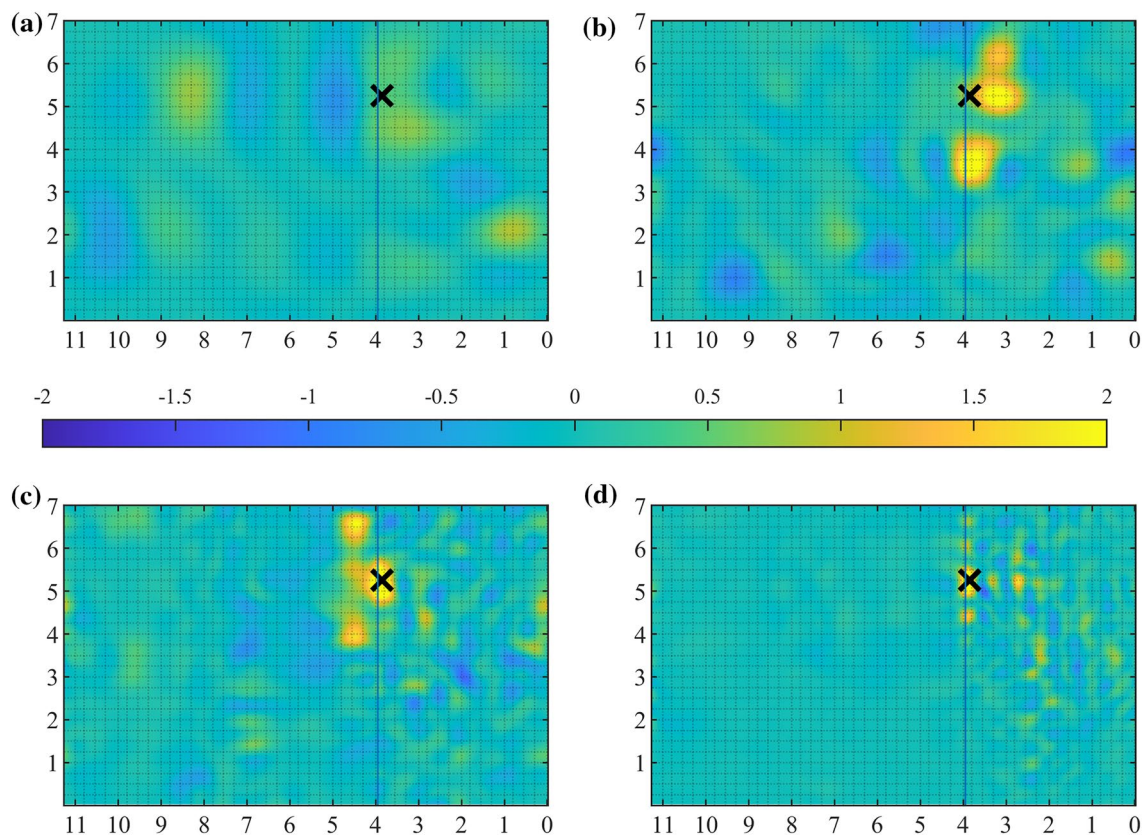


**Fig. 9** Perpendicularly directed time-averaged sound intensities in third octave bands with center frequencies **a** 63 Hz **b** 100 Hz and **c** 160 Hz; **d** 250 Hz; two-dimensional view; the point of excitation is marked by a cross; color bar in units of  $[10^{-6} \text{ W/m}^2\text{V}^2]$

insulation material covering the primary structure and on floor panels up to a frequency of 300 Hz. The method is applied in a reflective acoustic environment, while keeping a reasonable measurement time of approximately one hour. This can be advantageous compared to other methods of sound source determination. The scenario presented is based on the assumptions that a single source is present, generating a stationary sound field. Even with that simplification locations of dominant sound sources vary depending on the frequency. Nevertheless, sound intensity maps in one-third octave bands can reveal the location of sound sources especially at higher frequencies where the structure allows a more local transmission of acoustic energy in the cabin.

**Acknowledgements** The authors thank Kai Simanowski and Tom Langmann from the University of the Federal Armed Forces Hamburg for preparing sound pressure measurements in the AFL in Sect. 2.2. Also, the authors thank René Winter and Simon Heyen from the German Aerospace Centre for providing the vibrometer measurement data in Sect. 4.1. This work is part of the Federal Aviation Research Programme (LuFoV-2, Ref. No. 20K1511G), supported by the German Federal Ministry for Economic Affairs and Energy.

**Author contributions** Not applicable.

**Funding** Open Access funding enabled and organized by Projekt DEAL. This work is part of the Federal Aviation Research Programme (LuFoV-2, Ref. No. 20K1511G), supported by the German Federal Ministry for Economic Affairs and Energy.

**Availability of data and material** Not applicable.

**Code availability** Not applicable.

## Declarations

**Conflict of interest** Not applicable.

**Open Access** This article is licensed under a Creative Commons Attribution 4.0 International License, which permits use, sharing, adaptation, distribution and reproduction in any medium or format, as long as you give appropriate credit to the original author(s) and the source, provide a link to the Creative Commons licence, and indicate if changes were made. The images or other third party material in this article are included in the article's Creative Commons licence, unless indicated otherwise in a credit line to the material. If material is not included in the article's Creative Commons licence and your intended use is not permitted by statutory regulation or exceeds the permitted use, you will

need to obtain permission directly from the copyright holder. To view a copy of this licence, visit <http://creativecommons.org/licenses/by/4.0/>.

## References

- Radon, J.: Über die Bestimmung von Funktionen durch ihre Integralwerte längs gewisser Mannigfaltigkeiten. *Akad. Wiss.* **69**, 262–277 (1917)
- Hadamard, J.: Lectures on Cauchy's problem in linear partial differential equations. Yale University Press, New Haven (1923)
- Gabor, D.: A new microscopic principle. *Nature* **161**, 777–778 (1948)
- Goodman, J.W.: Introduction to Fourier optics. McGraw-Hill, San Francisco (1968)
- Shewell, J.R., Wolf, E.: Inverse diffraction and a new reciprocity theorem. *J. Opt. Soc. Am.* **58**(12), 1596–1603 (1968)
- Mueller, R.K.: Acoustic holography. *Proc. IEEE* **59**(9), 1319–1335 (1971)
- Williams, E.G., Maynard, J.D., Skudrzyk, E.: Sound source reconstructions using a microphone array. *J. Acoust. Soc. Am.* **68**(1), 340–344 (1980)
- Williams, E.G.: Fourier acoustics. Academic Press, San Diego (1999)
- Bies, D.A.: Uses of anechoic and reverberant rooms for the investigation of noise sources. *Noise Control Eng.* **7**(3), 154–163 (1976)
- Maynard, J.D.: Acoustic holography for wideband, arbitrarily shaped noise sources. *J. Acoust. Soc. Am.* **84**(1), 171 (1988)
- Williams, E., Houston, B.: New Green functions for nearfield acoustical holography in aircraft fuselages. In Proceedings of the AIAA and CEAS Aeroacoustics Conference, State College, PA, USA, pp. 96–1703 (1996)
- Wang, Z., Wu, S.F.: Helmholtz equation-least-squares method for reconstructing the acoustic pressure field. *J. Acoust. Soc. Am.* **102**(4), 2020–2032 (1997)
- Yoon, S.H., Nelson, P.A.: Estimation of acoustic source strength by inverse methods: part II, experimental investigation of methods for choosing regularization parameters. *J. Sound Vib.* **233**(4), 665–701 (2000)
- Holland, K.R., Nelson, P.A.: An experimental comparison of the focused beamformer and the inverse method for the characterisation of acoustic sources in ideal and non-ideal acoustic environments. *J. Sound Vib.* **331**(20), 4425–4437 (2012)
- Merino-Martínez, R., et al.: A review of acoustic imaging methods using phased microphone arrays. *CEAS Aeronaut. J.* **10**, 197–230 (2019)
- Sarkissian, A.: Method of superposition applied to patch near-field acoustic holography. *J. Acoust. Soc. Am.* **118**(2), 671–678 (2005)
- Antoni, J.: A Bayesian approach to sound source reconstruction optimal basis, regularization, and focusing. *J. Acoust. Soc. Am.* **131**(4), 2873–2890 (2012)
- Ungnad, S., Sachau, D.: Interior near-field acoustic holography based on finite elements. *J. Acoust. Soc. Am.* **146**(3), 1758–1768 (2019)
- Jacobsen, F., Chen, X., Jaud, V.: A comparison of statistically optimized near field acoustic holography using single layer pressure-velocity measurements and using double layer pressure measurements. *J. Acoust. Soc. Am.* **123**, 1842–1845 (2008)
- Braikia, Y., Melon, M., Langrenne, C., Bavu, É., Garcia, A.: Evaluation of a separation method for source identification in small spaces. *J. Acoust. Soc. Am.* **134**(1), 323–331 (2013)
- Herdic, P.C., Houston, B.H., Marcus, M.H., Williams, E.G., Baz, A.M.: The vibro-acoustic response and analysis of a full-scale aircraft fuselage section for interior noise reduction. *J. Acoust. Soc. Am.* **117**(6), 3667–3678 (2005)
- Williams, E.G., Houston, B.H., Herdic, P.C., Raveendra, S.T., Gardner, B.: Interior near-field acoustical holography in flight. *J. Acoust. Soc. Am.* **108**(4), 1451–1463 (2000)
- Williams, E.G., Valdivia, N.P., Herdic, P.C., Klos, J.: Volumetric acoustic vector intensity imager. *J. Acoust. Soc. Am.* **120**(4), 1887–1897 (2006)
- Moondra, M.S.: Visualizing interior and exterior jet aircraft noise. Wayne State University Dissertations (2014)
- Pereira, A., Leclère, Q., Lamotte, L., Paillasseur, S., Bleanodonu, L.: Noise source identification in a vehicle cabin using an iterative weighted approach to the equivalent source method. In: Proceedings of the International Conference on Noise and Vibration Engineering, Leuven, Belgium, pp. 285–294 (2012)
- Wu, S.F., Moondra, M.S., Beniwal, R.: Analyzing panel acoustic contributions toward the sound field inside the passenger compartment of a full-size automobile. *J. Acoust. Soc. Am.* **137**(4), 2101–2112 (2015)
- Bi, C., Jing, W., Zhang, Y., Xu, L.: Patch nearfield acoustic holography combined with sound field separation technique applied to a non-free field. *Sci. China Phys. Mech. Astron.* **58**(2), 1–9 (2015)
- Zhang, J., Xiao, X., Sheng, X., Li, Z.: Sound source localisation for a high-speed train and its transfer path to interior noise. *Chin. J. Mech. Eng.* **32**(1), 1–16 (2019)
- Wandel, M., Grund, V., Biedermann, J.: Validierung eines vibro-akustischen Simulationsmodells einer Flugzeugstruktur im mittleren Frequenzbereich. In: Proceedings of DLRK, Friedrichshafen (2018)
- Morse, P.M., Ingard, K.U.: Theoretical acoustics. Princeton University Press, Princeton (1968)
- Biedermann, J., Winter, R., Norambuena, M., Böswald, M.: Classification of the mid-frequency range based on spatial Fourier decomposition of operational deflection shapes. In: Proceedings of the 24th International Congress on Sound and Vibration (2017)
- Baker, B., Copson, E.T.: The mathematical theory of Huygens' principle. University Press, Oxford (2003)
- Randall, R.B.: Frequency analysis. Brüel & Kjaer, Naerum (1987)
- Bathe, K.-J., Zimmermann P.: Finite element procedures: Prentice Hall (1996)
- Golub, G.H., Reinsch, C.: Singular value decomposition and least squares solutions. *Numer. Math.* **14**(5), 403–420 (1970)
- Greville, T.N.E.: The Pseudoinverse of a rectangular or singular matrix and its application to the solution of systems of linear equations. *SIAM Rev.* **1**, 38–43 (1959)
- Tikhonov, A.: Solutions of ill-posed problems. Halsted Press, Washington, New York (1977)
- Hansen, P.C., O'Leary, D.P.: The use of the L-curve in the regularization of discrete ill-posed problems. *SIAM* **14**(6), 1487–1503 (1993)
- Fahy, F.: Sound intensity. E & FN Spon, London (1995)

**Publisher's Note** Springer Nature remains neutral with regard to jurisdictional claims in published maps and institutional affiliations.